Editors' Suggestion

Infrared Interlayer Exciton Emission in MoS_2/WSe_2 Heterostructures

Ouri Karni,[1,*] Elyse Barré,[2] Sze Cheung Lau,[1] Roland Gillen,[3] Eric Yue Ma,[1,4] Bumho Kim,[5] Kenji Watanabe,[6] Takashi Taniguchi,[6] Janina Maultzsch,[3] Katayun Barmak,[7] Ralph H. Page,[1,4] and Tony F. Heinz[1,4,†]

[1]*Department of Applied Physics, Stanford University, Stanford, California, 94305, USA*
[2]*Department of Electrical Engineering, Stanford University, Stanford, California, 94305, USA*
[3]*Department Physik, Friedrich-Alexander-Universität Erlangen-Nürnberg, Staudstrasse 7, 91058 Erlangen, Germany*
[4]*SLAC National Accelerator Laboratory, Menlo Park, California, 94025, USA*
[5]*Department of Mechanical Engineering, Columbia University, New York, New York 10027, USA*
[6]*National Institute for Materials Science, 1-1 Namiki, Tsukuba, Ibaraki 305-0044, Japan*
[7]*Department of Applied Physics and Applied Mathematics, Columbia University, New York, New York 10027, USA*

We report light emission around 1 eV (1240 nm) from heterostructures of MoS_2 and WSe_2 transition metal dichalcogenide monolayers. We identify its origin in an interlayer exciton (ILX) by its wide spectral tunability under an out-of-plane electric field. From the static dipole moment of the state, its temperature and twist-angle dependence, and comparison with electronic structure calculations, we assign this ILX to the fundamental interlayer transition between the K valleys in this system. Our findings gain access to the interlayer physics of the intrinsically incommensurate MoS_2/WSe_2 heterostructure, including moiré and valley pseudospin effects, and its integration with silicon photonics and optical fiber communication systems operating at wavelengths longer than 1150 nm.

Introduction.—Heterobilayers of two different semiconducting transition metal dichalcogenide (TMDC) monolayers (MLs) of the MX_2 family (with $M =$ Mo, W; $X = S$, Se) have recently been the subject of intense research. These studies are motivated both by probing the novel electronic and optical properties of these systems and by their potential for diverse device applications. As MLs, TMDCs exhibit strong light-matter interactions [1–5], dominated by tightly bound excitonic states [6]. Their stacking results in a rich variety of new physical processes, including ultrafast charge, spin, valley, and energy transfer [7], effects associated with the relative crystallographic orientation (twist angle) between the layers, such as moiré patterns [8–15] and, importantly, the emergence of interlayer exciton (ILX) states [16]. In such ILXs, an electron in one monolayer is bound to a hole in the other, separated by the van der Waals interlayer separation $t_{vdW} \approx 0.65$ nm [11]. Produced by efficient charge- and valley-transfer processes [17] and exhibiting long population [18] and valley [19,20] lifetimes, these ILXs could be key components for future applications of such heterostructures in (spin, valley, and optical) information processing and energy conversion. ILX light emission has been the subject of several recent investigations, primarily in $MoSe_2/WSe_2$ heterostructures [14–16,21–23], which emit in the 870–940 nm (1.32–1.42 eV) range. Importantly, it has been demonstrated that due to their static dipole moment, the emission energy of such ILXs is tunable by means of out-of-plane electric field [21,23], thus establishing a signature of ILX emission that distinguishes it from other intralayer or defect-related states. Together with theoretical work (e.g., Refs. [9,24]), the study of the $MoSe_2/WSe_2$ heterostructure has advanced the understanding of interlayer interactions in these systems. The wavelength range beyond 1150 nm, required for silicon photonics and optical fiber communications (OFC), has, however, remained inaccessible with this family of materials.

The MoS_2/WSe_2 heterostructure, the focus of the present investigation, differs from $MoSe_2/WSe_2$ by its significant mismatch in lattice constant (3.8% compared with just 0.3% [25]), and by its larger band offsets [25]. It has been examined as an electronic diode [26], a photovoltaic device [26,27], a photodiode [28], and as a light-emitting diode [29] in the visible range. However, the underlying nature of ILXs in this system has yet to be fully understood. ILX emission has been reported at wavelengths around 770 nm (1.6 eV) [30–32]. This energy lies above the interlayer energy gap (between the valence band edge in WSe_2 and the conduction band edge in MoS_2) inferred from scanning tunneling spectroscopy (STS) measurements [11,12], transport measurements [33], and predicted theoretically [25]. Hence, it is not compatible with an excitonic transition between those band edges. This discrepancy has been resolved by associating the observed emission at 770 nm with a *momentum-indirect* ILX, coupling the MoS_2 conduction-band edge with local minima in the WSe_2 valence band edge [31]. The nature of this state was revealed by demonstrating that the

corresponding emission exhibits only a weak twist-angle dependence and is suppressed at low temperatures [31]. Very recently, a lower-energy emission feature was reported at around 1120 nm in a nanocavity laser demonstration [34]. It was hypothesized to originate from an ILX [34], but without further investigating its properties or supplying direct evidence to confirm this assignment.

Here we show that the fundamental ILX, associated with band-edge states at the corners of the Brillouin zone (BZ) of the constituent layers (K/-K valleys), does indeed emit at a longer wavelength, around 1240 nm (1.0 eV). We prove this by demonstrating the linear Stark effect tuning associated by the large electric-dipole moment of the ILX [21,23]; under the application of a static out-of-plane electric field, we observe tuning over a range of 80 meV (90 nm). The inferred magnitude of the electric-dipole moment of the ILX also reflects the localization of the electron and hole wave functions in opposite layers of the heterostructure, characteristic of the K/-K valley states. This momentum-space configuration of the observed ILX is further identified through measurements of the dependence of the ILX emission on temperature and relative crystallographic alignment of the two layers (twist angle), as well as through electronic band-structure calculations. The elucidation of the basic electronic or optical properties of this model 2D heterostructure opens a pathway to explore the rich underlying physics of these intrinsically incommensurate heterostructures, such as the coupling of the valley pseudospin degree of freedom in the two layers and the influence of moiré patterns. Further, the observation of the fundamental ILX in this system will facilitate the combination of the optoelectronic functionality of 2D heterostructures with silicon photonics and with optical fiber communication in the O band (1260–1360 nm).

Results.—Electronic structure calculations: We have performed *ab initio* calculations to predict the energy of the fundamental ILX associated with the K/-K points of the BZ of the two constituent layers. Density functional theory (DFT) was used with GW corrections to determine the quasiparticle bands of a slightly stretched MoS_2/WSe_2 structure, as described in Supplemental Material S1 [35]. In Figs. 1(a)–1(b), we present the calculated unfolded DFT band structure of each layer in the heterostructure, which is the basis of the calculation of the K-K and K-Γ interlayer energy gaps. The results indicate that the smallest interlayer gap appears between the K points in both materials, between the WSe_2 valence band and the MoS_2 conduction band, reflecting a type-II band alignment consistent with previous measurements [11,12,20,26,52]. Based on an estimated ILX binding energy of 0.3 eV [24,53], we predict the energy of the ILX to be around 1.0–1.1 eV, with an electron residing at the K/-K valley in MoS_2 and a hole at the K/-K valley in WSe_2.

The momentum indirect K-Γ transitions are expected to lie at significantly higher energies, consistent with previous
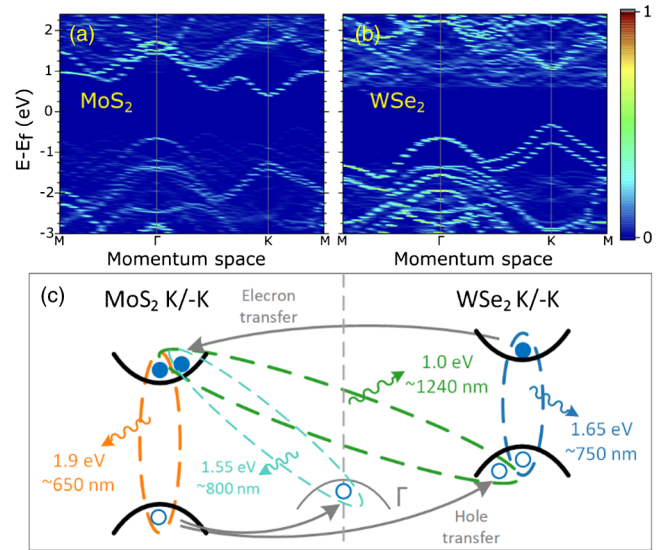

FIG. 1. Theoretical description of the electronic structure of the MoS_2/WSe_2 heterostructure. (a) The calculated band structure (at the DFT level of theory) unfolded onto the primitive BZ of MoS_2. The color represents the degree of localization of states within the MoS_2 layer (light green, yellow, and red indicate stronger localization of the band states in the layer.) (b) The same for the WSe_2 layer. (c) Schematic representation of the band alignment in a MoS_2/WSe_2 heterostructure. The configuration for the momentum-direct fundamental exciton investigated in this work is shown by the dashed dark green oval. The momentum-indirect exciton involving the Γ point, where the states are hybridized across the layers, is indicated by the teal oval. The arrows show charge transfer processes leading to the formation of the ILXs.

reports [31]. In addition, the calculation [Figs. 1(a)–1(b)] shows the hybridization of the nearly degenerate valence band states in the two layers around Γ, consistent with previous reports about $MoSe_2$/WSe_2 and MoS_2/graphene heterostructures [54–57]. In the MoS_2/WSe_2 system, hybridization of states at the Γ point renders the K-Γ transition a mixed inter- or intralayer transition, yielding an ILX with a reduced static electric-dipole moment. The electronic states in K/-K valleys, which are relevant for the fundamental ILX, are shown to be fully localized in the different layers (bright colors along the band of either WSe_2 or MoS_2, but not both). Hence, they are expected to produce an ILX with a dipole moment of $p \cong t_{vdW}e$, with e representing the elementary charge. The resulting band alignment, and excitonic emission energies (of both intra- and interlayer excitons) are summarized in Fig. 1(c). The intralayer excitons in isolated MoS_2 and WSe_2 monolayers have energies around 1.9 and 1.65 eV, respectively, at room temperature. Upon optical excitation of intralayer excitons, charge transfer [curved arrows in Fig. 1(c)] leads to the rapid creation of ILXs and the strong quenching of intralayer exciton photoluminescence (PL). It also supports the formation of the previously reported momentum-indirect exciton, with an energy around 1.6 eV (dashed teal oval), which involves the hybridized Γ-valley states of WSe_2

valence band (gray arc) [31]; the lowest-energy ILX as identified in this work, with both the electron and hole in the K/-K valleys, is designated by the dashed dark green oval.

Observation of infrared emission: For our experimental studies, several MoS_2/WSe_2 heterostructures were fabricated, both with and without encapsulation by insulating hexagonal boron nitride (hBN) layers. Some of the encapsulated samples were also equipped with top and bottom graphite gate electrodes. Thin flakes of graphite (DragonScale), hBN (National Institute for Material Science, Japan), and MLs of WSe_2 (HQ Graphene and Columbia University, USA) and MoS_2 (2D Semiconductors) were exfoliated from bulk crystals on polydimethylsiloxane (PDMS) stamps. The TMDC MLs were identified based on their optical contrast and PL. Subsequently, the heterostructures were stacked layer by layer using a dry-transfer technique [58], with each step followed by vacuum annealing at $150\,°C$ for 2 h. The crystallographic axes of the TMDCs were aligned judging by their sharp edges, yielding an alignment of the layers within a few degrees around $0°$ or $180°$. Electrical contacts to the semiconducting layers were realized by transferring elongated graphite flakes, to which we made electrical contact by evaporated metal layers patterned by electron-beam lithography. The thickness of hBN encapsulating layers, required for the modeling of the gating electric fields, was determined by atomic force microscopy. The optical measurements were performed in vacuum in a cryostat at temperatures between 20 and 295 K.

The visible and infrared (IR) PL spectra of the heterostructures were examined using a confocal microscope system (excitation spot size ~1 μm) and a spectrometer (Jobin Yvon iHR550) equipped with both a silicon CCD camera (Synapse) and an InGaAs array (Spectrum One), capable of measuring visible and 900–1700 nm light, respectively.

Figure 2(a) compares the room-temperature PL spectra from the isolated MLs and from the MoS_2/WSe_2 hetero-structure for hBN-encapsulated sample E1. We used excitation at 532 nm and 633 nm for measurements in the visible and IR ranges, respectively, with an intensity of $170\ W/cm^2$. As expected from their staggered band alignment [Fig. 1(c)], the PL associated with the monolayers in the visible spectral range is strongly quenched in the heterostructure due to rapid charge transfer processes. In the IR range, however, we observe pronounced emission at 0.97 eV (which shifts to an energy of 1.02–1.05 eV at cryogenic temperatures). The experimental data have been calibrated so that the vertical scale can be compared across the full spectral range (see Supplemental Material S2 [35]). A broad and weak background around 1.1 eV associated with emission from the silicon substrate [59] was subtracted from the traces. A microscope image of sample E1 is presented in Fig. 2(b). The inset shows a spatial map of the emission at 20 K in the spectral region around 1.0 eV,
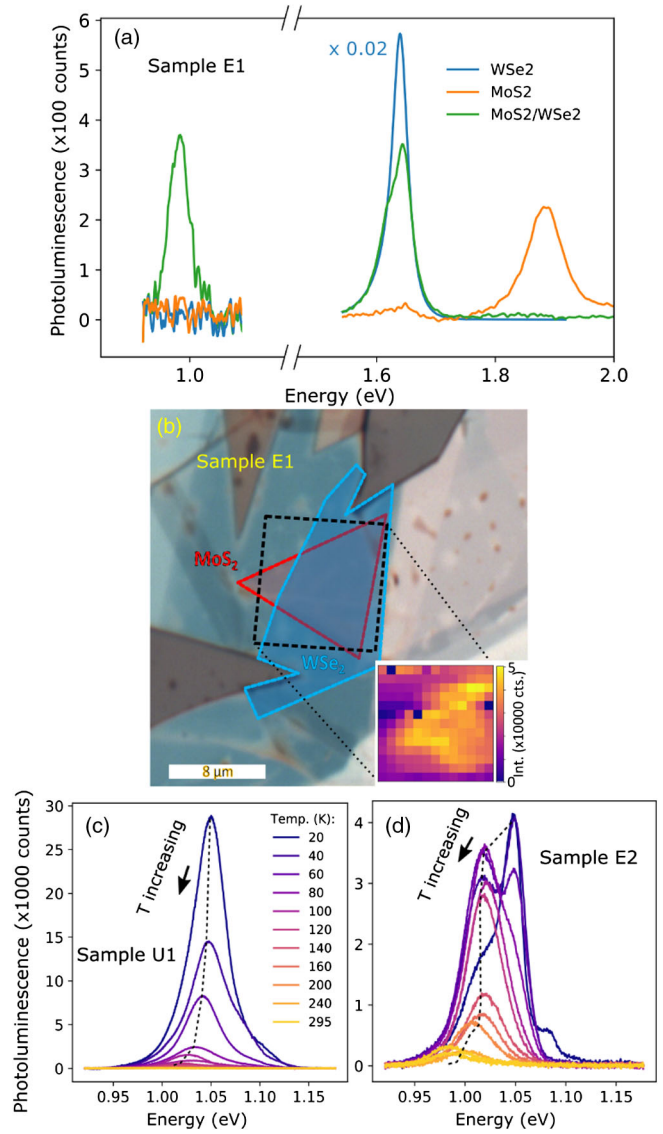

FIG. 2. Infrared emission of the MoS_2/WSe_2 heterostructure. (a) Room-temperature PL spectra for isolated MoS_2 and WSe_2 monolayers compared with the heterostructure in both the visible and IR ranges. Emission from WSe_2 (blue) is scaled down by a factor of 50 for comparison with the other spectra. The intensity scale applies for both visible and IR spectral ranges. (b) Microscope image of the corresponding heterostructure. The red, blue, and dashed black boundaries, respectively, delineate the MoS_2 ML, the WSe_2 ML, and the region of the spatial map of the 1200–1250 nm IR emission shown in the inset. (c) Temperature dependent PL spectra for unencapsulated sample U1. Temperatures range from 20 to 295 K, as indicated. (d) The same for encapsulated sample E2.

obtained using galvanometrically controlled mirrors to scan across the sample. We find that the IR emission is observed across the entire heterostructure region but is not seen from either ML separately.

The identified emission peak around 1.0 eV is very robust. Figures 2(c)–2(d) show, respectively, IR emission

spectra of unencapsulated sample U1 and encapsulated sample E2 (both supported on the same quartz substrate) and taken at various temperatures from 20 to 295 K (for excitation at 633 nm, 890 W/cm^2). Emission from the encapsulated sample E2 is observable at room temperature and increases in strength with decreasing temperature (see Supplemental Material S3 for similar behavior of sample E1 [35]). The emission from sample U1 also grows with decreasing temperature. We attribute the increased emission at reduced temperature to the expected growth in the fraction of ILXs with momenta that are small enough to allow radiative recombination, potentially in combination with some localization effect that helps to bridge the 3.8% of momentum mismatch between the band extrema, as discussed below [60,61].

The widths of the emission lines, which are as broad as 30–50 meV even at low temperatures, and their multipeak structure suggest the presence of spatial inhomogeneity in the ILX energy. Spatial modulation of the ILX energy is expected from the moiré pattern arising from the incommensuration of lattices of the two monolayers [14], perhaps also influenced by sample imperfections and defects. Evidence for spatial localization of the ILXs is provided by excitation-intensity dependent PL studies (Supplemental Material S4 [35]). These measurements show signatures of PL saturation with increasing intensity, as well as modification in the relative intensities of the various peaks. The results are compatible with the behavior expected for spatially confined ILXs, with their reduced density of states, rather than with additional peaks arising, for example, from exciton-phonon coupling [62]. Further, lateral confinement of the ILX should broaden its distribution in momentum space to accommodate the momentum mismatch between the MoS$_2$ CB minimum and WSe$_2$ VB maximum to achieve efficient radiative recombination at low temperatures. The apparent blueshift of the emission peak with increasing excitation intensity has been attributed to charge-transfer-induced changes to the band offset [63] or to dipole-dipole repulsion between ILXs [23,64] (which can be enhanced by a localizing potential, but is not expected to result in multi-peaked spectrum on its own). Further insight into the nature of the fine structure of the ILX spectrum and its relation to moiré effects should emerge from further study of the dependence of the ILX emission spectra on twist angle, temperature, excitation intensity, and optical polarization.

Electrical tunability of the ILX emission energy: To show unequivocally the interlayer nature of the emitting state, we examine the spectral tunability of the emission under the application of an electric field perpendicular to the plane of the heterostructure. The structure used for these measurements (sample E3) consists of a MoS$_2$/WSe$_2$ heterostructure encapsulated by insulating hBN layers, sandwiched between transparent conducting graphite gates [Fig. 3(a)]. This configuration allows us to apply modest
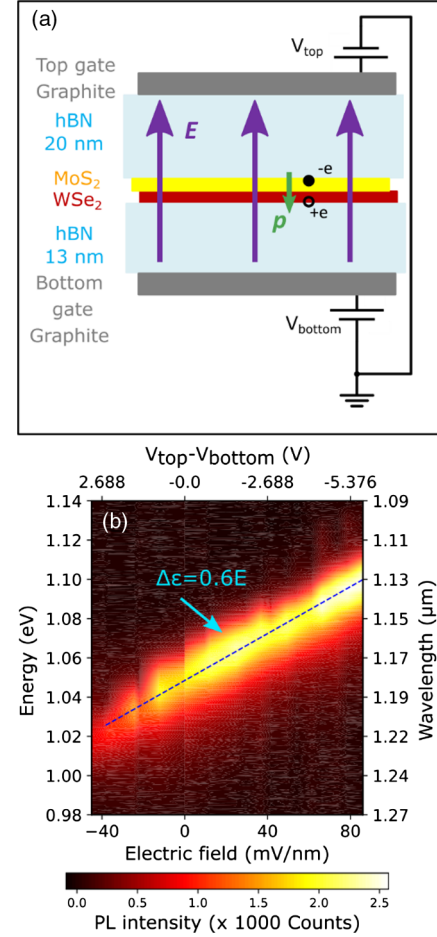

FIG. 3. (a) Schematic representation of the gated device used to apply an out-of-plane electric field to the MoS$_2$/WSe$_2$ heterostructure. The electron-hole pair of the ILX, split between the two different layers, gives rise to a static electric-dipole moment (green arrow) that is responsible for a linear Stark shift of the exciton energy under an applied electric field (purple arrows). (b) False-color map of the PL spectra measured as a function of voltage applied between the gates (top horizontal axis) and the corresponding electric field strength (bottom horizontal axis) within the heterostructure. The left and right vertical axes are the corresponding emission energy and wavelength. The dashed line shows a linear fit to the emission energy with applied electric field. The slope yields a dipole moment $p = 0.6\,e\,$nm.

and opposite bias voltages to the gates (up to ±3.5 V) to produce large electric fields across the heterostructure with minimal charge injection. Figure 3(b) presents the measured evolution of the IR PL spectrum (at 20 K, 470 W/cm^2 excitation intensity at 633 nm) as a function of voltage difference between the gates (top horizontal axis). The corresponding electric field E in the heterostructure (bottom horizontal axis) was calculated using previously reported out-of-plane dielectric constants for the TMDCs and the hBN layers (Supplemental Material S5 [35]). We observe strong and linear tuning of the ILX emission energy. The tuning range of ∼80 meV for the ILX

is limited on the negative side by the emergence of undesired charging effects, as discussed in Supplemental Material S6 [35]. In contrast, emission from the intralayer excitons, arising from states without an electric-dipole moment, exhibits no observable shift in energy with applied electric field.

We extract the shift of the ILX energy as a function of the applied field from Gaussian fits to the emission spectra. The resulting tuning of the ILX energy with bias voltage reflects the linear Stark effect, as expected for a charge separated ILX state possessing a finite electric-dipole moment p. The energy of the ILX transition should then vary with the applied electric field E as $\Delta \varepsilon = -p \cdot E$. By fitting the slope of the experimental ILX tuning curve, we infer a dipole moment of $p = 0.6 \pm 0.01\, e\,\mathrm{nm}$, pointing towards the WSe$_2$ layer [Fig. 3(a)]. Accounting for the uncertainty in the dielectric constants of the materials in the structure (Supplemental Material S5 [35]), we obtain an ILX dipole moment of $p = 0.5$–$0.8\, e\,\mathrm{nm}$. This value matches that expected for an ILX consisting of an electron located in the MoS$_2$ monolayer and the hole located in WSe$_2$ monolayer, separated from one another by the full interlayer spacing of approximately 0.65 nm [11]. Such strong field tuning of the feature is incompatible with emission from a state localized in either ML or at the interface and directly proves the interlayer character of the state. The wide electrical tunability of the emission in the IR is also, we note, attractive for diverse photonics applications.

Discussion.—The experimental results presented above provide direct evidence for the identification of a new ILX state lying in the infrared, far below the optical gap of each of the constituent MLs. Its gate tunability further reveals an electric-dipole moment corresponding to charge separation across the two layers, as expected for an interlayer state. The observed emission energy is also compatible with our theoretical study of the expected lowest energy ILX state. This indicates that the new ILX state identified here involves an electron in the K (or -K) valley of MoS$_2$ and a hole in the K (or -K) valley of WSe$_2$. This momentum-space assignment of the ILX state is also supported by additional experimental observations. First, the large ILX dipole moment deduced from the Stark effect measurements is expected for the layer-localized electrons and holes as they exist near the K and -K points [11,25], as opposed to other momentum-space states (e.g., the Γ or Σ points) that should experience significant interlayer hybridization. Second, to further confirm the momentum-direct character of the ILX states, we prepared and examined a few samples with intentionally misaligned crystallographic orientations; they showed almost no IR emission (Supplemental Material S7 [35]), consistent with the expected sensitivity to lattice alignment for radiative recombination of a momentum-direct ILX [61]. Finally, our temperature dependence measurements, showing enhanced emission at low temperatures, suggest that the observed ILX involves the band

edges, located at the K and -K points of the BZ, like the well-documented ILX of MoSe$_2$/WSe$_2$ heterostructures [16]. Altogether, this ILX completes the interlayer exciton spectrum of MoS$_2$/WSe$_2$ heterobilayers, so far investigated only for momentum-indirect ILX (coupling the K and the Γ points of the BZs) at a much higher energy.

From the perspective of photonics applications, the demonstrated gate tunability of the ILX has been shown to provide emission energies varying by more than 80 meV (90 nm) around 1.05 eV (1180 nm). This energy range lies just below the silicon band gap of 1.1 eV (1130 nm) at room temperature and 1.17 eV (1060 nm) at 20 K [65]. The MoS$_2$/WSe$_2$ heterostructure thus functions as a tunable nanoscale light source compatible with silicon photonics and close to the 1260–1360 nm OFC O band. This opens new possibilities. We expect, for example, that a MoS$_2$/WSe$_2$ p–n diode could be used as an electroluminescent light source for these platforms [28,29]. Alternatively, the highly tunable MoS$_2$/WSe$_2$ heterostructure could serve to modulate optical signals by tuning the transition in and out of resonance with the signal spectrum or with the modes of a microcavity system [34,66]. The tuning range demonstrated in these initial devices can be further extended if charge leakage is reduced, possibly by employing thicker hBN insulation to mitigate the defect assisted tunneling [67] (see Supplemental Material S6 [35]). Realizing the intrinsic breakdown strength of hBN of 1–1.2 V/nm [68] would allow us to apply electric fields as large as ~0.5 V/nm in the TMDC heterostructure. Based on our experimental results, we would then expect a tuning range reaching ± 300 meV. This extremely broad tuning would fully encompass the OFC O band around 1300 nm (0.95 eV) and the S and C bands around 1550 nm (0.7 eV).

In conclusion, we observed the fundamental ILX emission from aligned MoS$_2$/WSe$_2$ heterobilayers at around 1200 nm wavelength (1 eV energy). The significant dipole moment of the ILX results in strong electrical tunability of its emission energy. Based on the experimentally determined value of the ILX dipole moment, the strong twist-angle and temperature dependence of the emission, and the agreement with our band structure calculations, we have established that the state is associated with the K valleys of the constituent monolayers. This discovery should facilitate study of the effect of the lattice mismatch on the diverse properties of the ILXs, such as their spin or valley configuration, moiré modulation of their characteristics, [14,15] and the resulting correlation and topological effects [9,10]. In conjunction with the attractive wavelength of the ILX for optical fiber and silicon technologies, this new state also opens the door for coupling the above phenomena with photonic applications.

*Corresponding author.
oulrik@gmail.com
†Corresponding author.
tony.heinz@stanford.edu

[1] K. F. Mak, C. Lee, J. Hone, J. Shan, and T. F. Heinz, Phys. Rev. Lett. **105**, 136805 (2010).

[2] A. Splendiani, L. Sun, Y. Zhang, T. Li, J. Kim, C.-Y. Chim, G. Galli, and F. Wang, Nano Lett. **10**, 1271 (2010).

[3] C. Zhang, H. Wang, W. Chan, C. Manolatou, and F. Rana, Phys. Rev. B **89**, 205436 (2014).

[4] Y. Zhou, G. Scuri, J. Sung, R. J. Gelly, D. S. Wild, K. De Greve, A. Y. Joe, T. Taniguchi, K. Watanabe, P. Kim, M. D. Lukin, and H. Park, arxiv:1901.08500.

[5] C. Rogers, D. Gray, Jr., N. Bogdanowicz, T. Taniguchi, K. Watanabe, and H. Mabuchi, arxiv:1902.05036.

[6] A. Chernikov, T. C. Berkelbach, H. M. Hill, A. Rigosi, Y. Li, O. B. Aslan, D. R. Reichman, M. S. Hybertsen, and T. F. Heinz, Phys. Rev. Lett. **113**, 076802 (2014).

[7] C. Jin, E. Y. Ma, O. Karni, E. C. Regan, F. Wang, and T. F. Heinz, Nat. Nanotechnol. **13**, 994 (2018).

[8] E. M. Alexeev, D. A. Ruiz-Tijerina, M. Danovich, M. J. Hamer, D. J. Terry, P. K. Nayak, S. Ahn, S. Pak, J. Lee, J. I. Sohn, M. R. Molas, M. Koperski, K. Watanabe, T. Taniguchi, K. S. Novoselov, R. V. Gorbachev, H. S. Shin, V. I. Fal'ko, and A. I. Tartakovskii, Nature (London) **567**, 81 (2019).

[9] F. Wu, T. Lovorn, and A. H. MacDonald, Phys. Rev. Lett. **118**, 147401 (2017).

[10] H. Yu, G.-B. Liu, J. Tang, X. Xu, and W. Yao, Sci. Adv. **3**, e1701696 (2017).

[11] C. Zhang, C.-P. Chuu, X. Ren, M.-Y. Li, L.-J. Li, C. Jin, M.-Y. Chou, and C.-K. Shih, Sci. Adv. **3**, e1601459 (2017).

[12] Y. Pan, S. Fölsch, Y. Nie, D. Waters, Y.-C. Lin, B. Jariwala, K. Zhang, K. Cho, J. A. Robinson, and R. M. Feenstra, Nano Lett. **18**, 1849 (2018).

[13] C. Jin, E. C. Regan, A. Yan, M. I. B. Utama, D. Wang, S. Zhao, Y. Qin, S. Yang, Z. Zheng, S. Shi, K. Watanabe, T. Taniguchi, S. Tongay, A. Zettl, and F. Wang, Nature (London) **567**, 76 (2019).

[14] K. Tran *et al.*, Nature (London) **567**, 71 (2019).

[15] K. L. Seyler, P. Rivera, H. Yu, N. P. Wilson, E. L. Ray, D. G. Mandrus, J. Yan, W. Yao, and X. Xu, Nature (London) **567**, 66 (2019).

[16] P. Rivera, H. Yu, K. L. Seyler, N. P. Wilson, W. Yao, and X. Xu, Nat. Nanotechnol. **13**, 1004 (2018).

[17] J. R. Schaibley, P. Rivera, H. Yu, K. L. Seyler, J. Yan, D. G. Mandrus, T. Taniguchi, K. Watanabe, W. Yao, and X. Xu, Nat. Commun. **7**, 13747 (2016).

[18] P. Rivera, J. R. Schaibley, A. M. Jones, J. S. Ross, S. Wu, G. Aivazian, P. Klement, K. Seyler, G. Clark, N. J. Ghimire, J. Yan, D. G. Mandrus, W. Yao, and X. Xu, Nat. Commun. **6**, 6242 (2015).

[19] P. Rivera, K. L. Seyler, H. Yu, J. R. Schaibley, J. Yan, D. G. Mandrus, W. Yao, and X. Xu, Science **351**, 688 (2016).

[20] J. Kim, C. Jin, B. Chen, H. Cai, T. Zhao, P. Lee, S. Kahn, K. Watanabe, T. Taniguchi, S. Tongay, M. F. Crommie, and F. Wang, Sci. Adv. **3**, e1700518 (2017).

[21] A. Ciarrocchi, D. Unuchek, A. Avsar, K. Watanabe, T. Taniguchi, and A. Kis, Nat. Photonics **13**, 131 (2019).

[22] A. T. Hanbicki, H.-J. Chuang, M. R. Rosenberger, C. S. Hellberg, S. V. Sivaram, K. M. McCreary, I. I. Mazin, and B. T. Jonker, ACS Nano **12**, 4719 (2018).

[23] L. A. Jauregui, A. Y. Joe, K. Pistunova, D. S. Wild, A. A. High, Y. Zhou, G. Scuri, K. De Greve, A. Sushko, C.-H. Yu, T. Taniguchi, K. Watanabe, D. J. Needleman, M. D. Lukin, H. Park, and P. Kim, arxiv:1812.08691.

[24] R. Gillen and J. Maultzsch, Phys. Rev. B **97**, 165306 (2018).

[25] C. Zhang, C. Gong, Y. Nie, K.-A. Min, C. Liang, Y. J. Oh, H. Zhang, W. Wang, S. Hong, L. Colombo, R. M. Wallace, and K. Cho, 2D Mater. **4**, 015026 (2017).

[26] C.-H. Lee, G.-H. Lee, A. M. van der Zande, W. Chen, Y. Li, M. Han, X. Cui, G. Arefe, C. Nuckolls, T. F. Heinz, J. Guo, J. Hone, and P. Kim, Nat. Nanotechnol. **9**, 676 (2014).

[27] M. M. Furchi, A. Pospischil, F. Libisch, J. Burgdörfer, and T. Mueller, Nano Lett. **14**, 4785 (2014).

[28] R. Cheng, D. Li, H. Zhou, C. Wang, A. Yin, S. Jiang, Y. Liu, Y. Chen, Y. Huang, and X. Duan, Nano Lett. **14**, 5590 (2014).

[29] O. L. Sanchez, D. Ovchinnikov, S. Misra, A. Allain, and A. Kis, Nano Lett. **16**, 5792 (2016).

[30] H. Fang, C. Battaglia, C. Carraro, S. Nemsak, B. Ozdol, J. S. Kang, H. A. Bechtel, S. B. Desai, F. Kronast, A. A. Unal, G. Conti, C. Conlon, G. K. Palsson, M. C. Martin, A. M. Minor, C. S. Fadley, E. Yablonovitch, R. Maboudian, and A. Javey, Proc. Natl. Acad. Sci. U.S.A. **111**, 6198 (2014).

[31] J. Kunstmann, F. Mooshammer, P. Nagler, A. Chaves, F. Stein, N. Paradiso, G. Plechinger, C. Strunk, C. Schüller, G. Seifert, D. R. Reichman, and T. Korn, Nat. Phys. 14, 801 (2018).

[32] D. Unuchek, A. Ciarrocchi, A. Avsar, K. Watanabe, T. Taniguchi, and A. Kis, Nature (London) 560, 340 (2018).

[33] E. Ponomarev, N. Ubrig, I. Gutiérrez-Lezama, H. Berger, and A. F. Morpurgo, Nano Lett. 18, 5146 (2018).

[34] Y. Liu, H. Fang, A. Rasmita, Y. Zhou, J. Li, T. Yu, Q. Xiong, N. Zheludev, J. Liu, and W. Gao, Sci. Adv. 5, eaav4506 (2019).

[35] See Supplemental Material at http://link.aps.org/supplemental/10.1103/PhysRevLett.123.247402 for supporting computational and experimental details, which includes Refs. [36–51].

[36] P. Giannozzi et al., J. Phys. Condens. Matter 21, 395502 (2009).

[37] D. R. Hamann, Phys. Rev. B 88, 085117 (2013).

[38] P. V. C. Medeiros, S. Stafström, and J. Björk, Phys. Rev. B 89, 041407 (2014).

[39] P. V. C. Medeiros, S. S. Tsirkin, S. Stafström, and J. Björk, Phys. Rev. B 91, 041116 (2015).

[40] J. E. Moussa, P. A. Schultz, and J. R. Chelikowsky, J. Chem. Phys. 136, 204117 (2012).

[41] K. Kim, S. Larentis, B. Fallahazad, K. Lee, J. Xue, D. C. Dillen, C. M. Corbet, and E. Tutuc, ACS Nano 9, 4527 (2015).

[42] S. K. Jang, J. Youn, Y. J. Song, and S. Lee, Sci. Rep. 6, 30449 (2016).

[43] O. Ciftja, RSC Adv. 9, 7849 (2019).

[44] G. Shi, Y. Hanlumyuang, Z. Liu, Y. Gong, W. Gao, B. Li, J. Kono, J. Lou, R. Vajtai, P. Sharma, and P. M. Ajayan, Nano Lett. 14, 1739 (2014).

[45] L. H. Li, E. J. G. Santos, T. Xing, E. Cappelluti, R. Roldán, Y. Chen, K. Watanabe, and T. Taniguchi, Nano Lett. 15, 218 (2015).

[46] Z. Wang, L. Zhao, K. F. Mak, and J. Shan, Nano Lett. 17, 740 (2017).

[47] K. K. Kim, A. Hsu, X. Jia, S. M. Kim, Y. Shi, M. Dresselhaus, T. Palacios, and J. Kong, ACS Nano 6, 8583 (2012).

[48] J. A. Wilson and A. D. Yoffe, Adv. Phys. 18, 193 (1969).

[49] E. Courtade, M. Semina, M. Manca, M. M. Glazov, C. Robert, F. Cadiz, G. Wang, T. Taniguchi, K. Watanabe, M. Pierre, W. Escoffier, E. L. Ivchenko, P. Renucci, X. Marie, T. Amand, and B. Urbaszek, Phys. Rev. B 96, 085302 (2017).

[50] A. F. Rigosi, H. M. Hill, Y. Li, A. Chernikov, and T. F. Heinz, Nano Lett. 15, 5033 (2015).

[51] M. Danovich, D. A. Ruiz-Tijerina, R. J. Hunt, M. Szyniszewski, N. D. Drummond, and V. I. Fal'ko, Phys. Rev. B 97, 195452 (2018).

[52] M.-H. Chiu, C. Zhang, H.-W. Shiu, C.-P. Chuu, C.-H. Chen, C.-Y. S. Chang, C.-H. Chen, M.-Y. Chou, and L.-J. Li, Nat. Commun. 6, 7666 (2015).

[53] S. Latini, K. T. Winther, T. Olsen, and K. S. Thygesen, Nano Lett. 17, 938 (2017).

[54] N. R. Wilson, P. V. Nguyen, K. Seyler, P. Rivera, A. J. Marsden, Z. P. L. Laker, G. C. Constantinescu, V. Kandyba, A. Barinov, N. D. M. Hine, X. Xu, and D. H. Cobden, Sci. Adv. 3, e1601832 (2017).

[55] A. Ebnonnasir, B. Narayanan, S. Kodambaka, and C. V. Ciobanu, Appl. Phys. Lett. 105, 031603 (2014).

[56] W. Jin, P.-C. Yeh, N. Zaki, D. Chenet, G. Arefe, Y. Hao, A. Sala, T. O. Mentes, J. I. Dadap, A. Locatelli, J. Hone, and R. M. Osgood, Phys. Rev. B 92, 201409 (2015).

[57] L. Du, H. Yu, M. Liao, S. Wang, L. Xie, X. Lu, J. Zhu, N. Li, C. Shen, P. Chen, R. Yang, D. Shi, and G. Zhang, Appl. Phys. Lett. 111, 263106 (2017).

[58] A. Castellanos-Gomez, M. Buscema, R. Molenaar, V. Singh, L. Janssen, H. S. J. van der Zant, and G. A. Steele, 2D Mater. 1, 011002 (2014).

[59] W. S. Yoo, K. Kang, G. Murai, and M. Yoshimoto, ECS J. Solid State Sci. Technol. 4, P456 (2015).

[60] C. Robert, D. Lagarde, F. Cadiz, G. Wang, B. Lassagne, T. Amand, A. Balocchi, P. Renucci, S. Tongay, B. Urbaszek, and X. Marie, Phys. Rev. B 93, 205423 (2016).

[61] H. Yu, Y. Wang, Q. Tong, X. Xu, and W. Yao, Phys. Rev. Lett. 115, 187002 (2015).

[62] Z. Li, T. Wang, C. Jin, Z. Lu, Z. Lian, Y. Meng, M. Blei, S. Gao, T. Taniguchi, K. Watanabe, T. Ren, S. Tongay, L. Yang, D. Smirnov, T. Cao, and S.-F. Shi, Nat. Commun. 10, 2469 (2019).

[63] E. Y. Ma, B. Guzelturk, G. Li, L. Cao, Z.-X. Shen, A. M. Lindenberg, and T. F. Heinz, Sci. Adv. 5, eaau0073 (2019).

[64] P. Nagler, G. Plechinger, M. V. Ballottin, A. Mitioglu, S. Meier, N. Paradiso, C. Strunk, A. Chernikov, P. C. M. Christianen, C. Schüller, and T. Korn, 2D Mater. 4, 025112 (2017).

[65] B. G. Streetman and S. Banerjee, Solid State Electronic Devices, 7th ed. (Pearson, Upper Saddle River, NJ, USA, 2015).

[66] M. Förg, L. Colombier, R. K. Patel, J. Lindlau, A. D. Mohite, H. Yamaguchi, M. M. Glazov, D. Hunger, and A. Högele, Nat. Commun. 10, 3697 (2019).

[67] L. Ju, J. Velasco, Jr., E. Huang, S. Kahn, C. Nosiglia, H.-Z. Tsai, W. Yang, T. Taniguchi, K. Watanabe, Y. Zhang, G. Zhang, M. Crommie, A. Zettl, and F. Wang, Nat. Nanotechnol. 9, 348 (2014).

[68] Y. Hattori, T. Taniguchi, K. Watanabe, and K. Nagashio, Appl. Phys. Lett. 109, 253111 (2016).